

Nanoscale

Accepted Manuscript



This is an *Accepted Manuscript*, which has been through the Royal Society of Chemistry peer review process and has been accepted for publication.

Accepted Manuscripts are published online shortly after acceptance, before technical editing, formatting and proof reading. Using this free service, authors can make their results available to the community, in citable form, before we publish the edited article. We will replace this *Accepted Manuscript* with the edited and formatted *Advance Article* as soon as it is available.

You can find more information about *Accepted Manuscripts* in the [Information for Authors](#).

Please note that technical editing may introduce minor changes to the text and/or graphics, which may alter content. The journal's standard [Terms & Conditions](#) and the [Ethical guidelines](#) still apply. In no event shall the Royal Society of Chemistry be held responsible for any errors or omissions in this *Accepted Manuscript* or any consequences arising from the use of any information it contains.

ARTICLE

Surface chemistry, morphological analysis and properties of cellulose nanocrystals with gradient sulfation degrees

Cite this: DOI: 10.1039/x0xx00000x

Ning Lin and Alain Dufresne*

Received 00th January 2012,
Accepted 00th January 2012

DOI: 10.1039/x0xx00000x

www.rsc.org/

The process of sulfuric acid-hydrolysis of cellulose fibers for the preparation of cellulose nanocrystals (CNs) includes an esterification reaction between acid and cellulose molecules, which induce the covalent coupling of sulfate groups on the surface of prepared CNs. Negatively charged sulfate groups play an important role in both surface chemistry and physical properties of CNs. This study explored the strategy of introducing a gradient of sulfate groups on the surface of CNs, and further investigated the effect of the sulfation degree on surface chemistry, morphology and dimension, and physical properties of different CNs samples. Based on the discussion of its surface chemistry, the selection of different cross-section models was reported to significantly affect the calculation of the degree of substitution of sulfate groups on CNs. A new ellipse cross-section model was proposed on the basis of AFM observation. The effect of sulfate groups on crystal properties and thermal stability was discussed and validated, and birefringence behavior of nanocrystal suspensions was observed.

Introduction

Despite being the most available natural polymer on earth, it is only quite recently that cellulose has gained prominence as a nanostructured material, in the form of cellulose nanocrystals (CNs) and nanofibrillated cellulose (NFC).¹ Cellulose nanocrystal is being developed for use over a broad range of applications, even if a high number of unknowns remain at date. After intensive studies, it was shown that the potential of CN focused on its mechanical properties as nano-reinforcing phase and advanced functional applications based on its special properties. The sound markets impacted by CNs include composites, electronics (flexible circuits), energy (flexible battery, such as Li-ion battery and solar panels), packaging, coatings, detergents, adhesives, construction, pulp and paper, inks and printing, filtration, medicine and life science (scaffolds in tissue engineering, artificial skin and cartilage, wound healing, and vessel substitutes), optical devices (including reflective properties for security papers and UV or IR reflective barriers), rheological modifiers, and cosmetics.^{1,2} Properties of cellulose nanocrystals, related materials, and potential foreshadowed applications have been extensively reviewed, and some recent review articles include preparation technologies,³ properties,⁴ nanocomposites,^{5,6} and functional materials.⁷⁻⁹

Common preparation of CN consists in an acid-induced destructuring process, during which the heterogeneous acid hydrolysis involves the diffusion of acid molecules into

cellulose fibers, and following cleavage of glycosidic bonds. Different strong acids have been shown to successfully degrade non-crystalline (amorphous) regions of cellulose fibers to release crystalline cellulosic nanoparticles, such as sulfuric, hydrochloric, phosphoric, hydrobromic, nitric acids, and a mixture composed of hydrochloric and organic acids.¹⁰ Nevertheless, the hydrolysis treatment with sulfuric acid to prepare CNs has been extensively investigated and appears to be the most effective method. One of the main reason for using sulfuric acid as a hydrolyzing agent is that if CNs are prepared using hydrochloric acid, their ability to disperse in solvents is limited and the suspension is unstable tending to flocculate. Indeed, during hydrolysis, sulfuric acid reacts with the surface hydroxyl groups via an esterification process allowing the grafting of anionic sulfate ester groups ($-OSO_3^-$).¹¹ These sulfate groups are randomly distributed on the surface of cellulosic nanoparticle. The presence of these negatively charged sulfate ester groups induces the formation of a negative electrostatic layer covering the surface of nanocrystals and promotes their dispersion in solvents. The high stability of sulfuric acid-hydrolyzed CNs results therefore from an electrostatic repulsion between individual nanoparticles.

Besides the promotion of high stability of nanocrystals in solvents, surface $-OSO_3^-$ groups with negative charges also provide CNs the accessibility for diverse functional applications via electrostatic adsorption, such as layer-by-layer

(LBL) assembling nanomaterials from anionic nanocrystals and cationic matrix;^{12,13} electrochemical nanocomposites with the process of electrochemical co-deposition;¹⁴ microfiltration membrane with high adsorption capacity against positively charged dye;¹⁵ permselective membranes from exclusion or adsorption for different charged molecules;¹⁶ and electrostatic adsorption of enzymes (cellulase) on enzymatic hydrolysis of substrates.¹⁷ Recently, it was reported that surface sulfate groups and charge density of CNs even play a significant role in the control of water/oil interface for emulsion stability.¹⁸

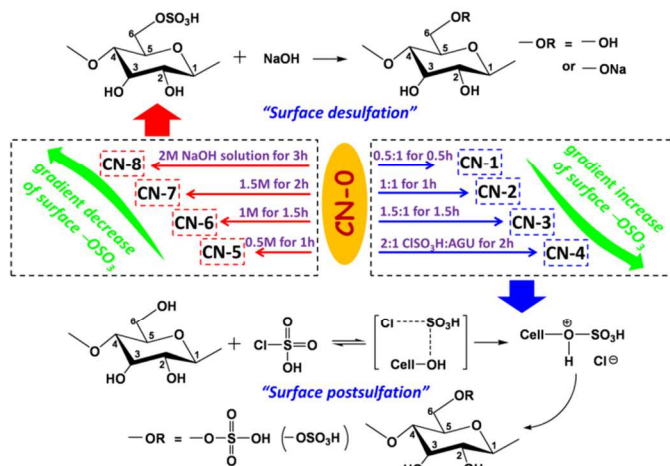


Fig. 1 Strategy of gradient introducing sulfate groups on the surface of H_2SO_4 -hydrolyzed cellulose nanocrystals.

The objectives of this study are to discuss the surface chemistry of sulfated cellulose nanocrystals, and further investigate the morphology and properties of nanocrystals with different contents of sulfate groups. Using postsulfation and desulfation treatments, a series of CNs (nine) samples behaving gradient degrees of sulfate groups were prepared through the regulation of reactant ratios and reactive conditions. Chlorosulfonic acid was used as sulfating agent for the postsulfation of CNs, which can provide higher levels of surface sulfation, and avoid the drawbacks of deep degradation of nanocrystals induced by strong sulfuric acid. Figure 1 shows the strategy and mechanism of introducing gradient sulfate groups on the surface of CNs. In addition, surface chemistry analysis for sulfated CN is a significant research point because of its crucial influence to subsequent surface modifications, especially the determination of surface degree of substitution (*DS*) of diverse grafted groups or molecules on nanocrystals. Several studies reported different *DS* values ranging from 1/10 to 1/3 or 1/2 of free hydroxyl groups replaced by sulfate groups for 65 wt% H_2SO_4 -hydrolyzed CNs.^{19,20} In this study, based on the comparison of four cross-section models (square, round, rectangle, ellipse), different effects to surface chemistry of CNs were analyzed and discussed. Moreover, surface sulfate groups should significantly affect physical properties of CNs or their suspensions, such as crystal properties, zeta-potential, thermal properties, and birefringence behavior. It should be noted that despite that some studies have reported the influence of

sulfation degree on thermal degradation of CNs, inconsistent conclusions were provided. For instance, in an earlier study, it was believed that the sulfate groups borne by CNs caused a significant decrease in degradation temperature, even at low levels.²¹ However, a recent study reported the slight increase of degradation temperature for higher levels of sulfated groups on CNs.²² In this study, besides the thermal degradation influence, various effects of sulfate groups to the physical properties of CNs will be further investigated and validated.

Experimental sections

Materials. Native cotton fibers were obtained from Whatman filter paper. Sulfuric acid (H_2SO_4 , 98%), chlorosulfonic acid (ClSO_3H), dimethylformamide (DMF), sodium hydroxide (NaOH) and other reagents were purchased from Sigma-Aldrich, and used without further treatment.

Extraction of CNs via sulfuric acid hydrolysis.

Cellulose nanocrystals (CNs) were prepared by H_2SO_4 hydrolysis of native cotton fiber, according to our previous protocol.²³ Cotton fiber was milled with a laboratory milling device to obtain a fine particulate substance. Acid hydrolysis was performed at 45 °C with 65 wt% H_2SO_4 (preheated) for 60 min under mechanical stirring (25.0 g fibers for 500 mL solution). The suspension was diluted with ice cubes to stop the reaction and washed until neutrality by successive centrifugations at 10,000 rpm (rotation per minute) for 10 min each step and dialyzed against distilled water for three days. Upon exhaustive dialysis treatment, free acid molecules were removed. CN suspension was dispersed by ultrasonic treatment using a Branson sonifier for three 5-min cycles (with cooling as necessary to prevent overheating). Finally, the released CN powder was obtained by freeze-drying.

Surface postsulfation of H_2SO_4 -hydrolyzed CNs.

Surface postsulfation was realized using chlorosulfonic acid (ClSO_3H) as sulfation agent to obtain sulfated CNs with different substitution degrees.^{24,25} About 3.0 g freeze-dried CN, with 18.53 mmol equivalent anhydroglucose unit (AGU), was suspended in 100 mL anhydrous DMF and ultrasonically dispersed with a Branson Sonifier for 5 min. The sulfation agent, a complex mixture of ClSO_3H and DMF, was prepared by slowly adding ClSO_3H into 50 mL anhydrous DMF with constant stirring and cooling in ice bath. (**Caution!** Chlorosulfonic acid is a strong corrosive and volatile chemical; thus, the mixing treatment should be handled in the fume hood with precaution and proper safety protection.) Sulfation of CN was initiated by gradually adding ClSO_3H into prepared nanocrystal suspension, with the regulation of reactant ratios between ClSO_3H and AGU ranging from 0.5 to 2.0 mol/mol, keeping vigorous stirring for 0.5–2.0 h at room temperature. The reaction was terminated by adding ethanol. The suspension was washed with anhydrous alcohol and exchanged to water, centrifuged and dialyzed against deionized water for three days. Finally, the products of sulfated CNs were obtained by freeze-drying treatment.

Surface desulfation of H₂SO₄-hydrolyzed CNs.

It was reported that two different treatments can be performed for the desulfation of CNs, viz. solvolytic desulfation,²⁶ and alkaline desulfation.^{27,28} In order to realize the desulfation gradient, alkaline (NaOH) desulfation approach was used to remove surface sulfate groups on CNs in this work. Different concentrations of alkaline solution (ranging from 0.5 to 2.0 mol/L) were added to the CN aqueous suspension, with the control of maximum alkaline concentration at 2 mol/L. In a typical procedure, 100 mL aqueous CN suspension (resulting CN concentration about 2 wt%) was mixed with 50 mL NaOH solution with given concentration, and the mixture was stirred at 60 °C for 1–3 h. During the reaction, cellulose nanoparticles in suspension gradually aggregated and settled in the bottom because of the removal of surface sulfate groups. With centrifugation and dialysis treatments, obtained suspension was purified, and finally the desulfated CNs powder was prepared by freeze-drying treatment.

On the basis of postsulfation and desulfation experiments, CNs samples possessing different contents of surface sulfate groups were named as CN-(0 to 8), as shown in the strategy depicted in Figure 1. In here, CN-0 represents the initial CN product hydrolyzed from 65 wt% sulfuric acid without further modification; CN-(1 to 4) are the further sulfated nanocrystals, and CN-(5 to 8) are desulfated nanocrystals obtained with different reactant ratios and reaction durations.

Characterization and Analysis.

Fourier Transform Infrared Spectroscopy (FTIR)

Infrared spectra were recorded at room temperature on a FTIR Perkin-Elmer Spectrum One spectrometer to characterize the surface postsulfation and desulfation of CNs. All freeze-dried samples were prepared as KBr pellets (1 wt% CN powder in anhydrous KBr), and analyzed using a spectral width ranging from 4000 to 400 cm⁻¹ with a 2 cm⁻¹ resolution and an accumulation of 32 scans.

X-ray Photoelectron Spectroscopy (XPS)

Surface postsulfation and desulfation of CNs (samples CN-0; CN-4; CN-8) were further analyzed by XPS following the signal of sulfur element (S) and sodium element (Na). The S/C and Na/C content ratios were calculated according to Eq. (1) from the XPS results. The experiments were carried out using an XR3E2 apparatus (Vacuum Generators, U.K.) equipped with an unmonochromated Mg KR X-ray source (1253.6 eV) and operated at 15 kV under a current of 20 mA. Samples were prepared as pastilles (10 mm diameter) and characterized in an ultrahigh vacuum chamber (10⁻⁸ mbar) with electron collection by a hemispherical analyzer at a 90° angle.

$$S/C = \frac{A_S}{N_S} \times \frac{N_C}{A_C} \quad (1)$$

Elemental analysis

Elemental analysis was used to determine the total content of sulfur element in CNs samples, and was performed at Analysis Central Service of the Centre National de la Recherche Scientifique (Vernaison, France). Before analysis, freeze-dried

samples were further treated under vacuum at room temperature for 8 h. The sulfur, carbon, and oxygen element contents were measured for postsulfated and desulfated CNs.

Morphology and dimensions

The morphology of CNs samples was observed using atomic force microscopy (AFM). Suspensions of approximately 0.01 wt% nanocrystals were dispersed in water with ultrasonic dispersion for 30 min and then deposited on the mica substrate. The substrate loaded with nanoparticles was imaged in tapping mode with a Nanoscope IIIa microscope from Veeco Instruments. Silicon cantilevers were used to perform the imaging at a frequency of 264–339 kHz and a typical radius of curvature of 10–15 nm.

The CNs dimensions, including length (*L*), width (*W*), and height (*H*), were measured by Nanoscope software. Over 100 rod-like nanocrystals were statistically analyzed to determine the average length, width, height and distribution.

Surface charge

The ζ-potential of CNs in water (0.01 wt%) was determined by a zeta-meter (Zetasizer DTS0230 Malvern Instruments). The instrument measures electrophoretic light scattering of a 35 mW solid state laser beam at a 660 nm wavelength, and all reported values were an average of 5 measurements with confidence intervals of 95%.

Crystal properties

The crystallinity index and crystalline dimensions in different planes of CNs were measured by X-ray diffraction analysis, in order to investigate the effect of surface sulfate groups to crystalline properties. The X-ray diffraction patterns were recorded on a Philips PW 1720 X-ray generator operated at 45 kV and 40 mA with Cu Kα radiation (λ = 0.154 nm) in the range 2θ = 5–50° for samples using a fixed time mode with a step interval of 0.066°. The crystallinity index (χ_c) of native cotton and CN was calculated according to Segal equation:

$$\chi_c = \frac{I_{200} - I_{am}}{I_{200}} \times 100\% \quad (2)$$

In Eq. (2), *I*₂₀₀ is the overall intensity of the peak at 2θ about 22.7°, and *I*_{am} represents the intensity of the baseline at 2θ about 18.0°.

Crystalline dimensions of different planes for CNs samples were calculated according to Scherrer equation:

$$B_{hkl} = \frac{0.9\lambda}{\beta_{1/2} \cos\theta} \quad (3)$$

In Eq. (3), *B*_{hkl} is the average crystalline width of a specific plane; λ represents the wavelength of incident X-rays (λ = 0.15418 nm); θ is the center of the peak; and β_{1/2} (in radius) represents the full width at half maximum (FWHM) of the reflection peak.

Thermal degradation

To investigate the effect of sulfate groups with different degrees of substitution on the thermal stability of CNs and native cotton, thermogravimetric analysis (TGA) was performed using a thermal analyzer Perkin-Elmer TGA-6 under air flow. Samples of ca. 10 mg were heated from 20 to 600 °C at a heating rate of 10 °C/min.

Birefringence behavior of suspensions

The suspension of lyophilized CNs was transferred to a 5 mL glass vial, and ultrasonicated for 30 min. The concentration of nanocrystals in suspension was controlled as about 0.5 wt%, which was used to observe the dispersion and birefringence between two crossed polarizers due to macroscopic anisotropy of rod-like nanoparticles. The presence of birefringence was used as the criterion of good dispersability or somewhat aggregation for nanoparticles in aqueous suspensions.²⁹

Results and discussion

Spectroscopy proofs for gradient sulfation of cellulose nanocrystals.

The main challenge for the chemical functionalization of cellulose nanocrystals (CNs) is to conduct a reaction taking place on the surface of nanocrystals, while preserving the original morphology and structure to avoid any polymorphic conversion and to maintain the integrity of the crystal.¹⁰ In this study, to realize the further surface sulfation of CNs, the duration and reactant ratio between sulfated agent and CN ($\text{ClSO}_3\text{H}:\text{AGU}$) are critical conditions. The addition of ClSO_3H was regulated as 0.5, 1.0, 1.5 or maximum 2.0 ratios according to the AGU of cellulose, and the reactions were performed for 0.5, 1.0, 1.5 and 2.0 h, respectively. Under these conditions, the desired achievement of sufficient substitution of hydroxyl groups to sulfated groups and preservation of original crystalline structure and geometrical morphology of nanocrystals can be realized, which will be proved by following characterizations and results. In fact, higher reaction ratios (such as 4:1 for $\text{ClSO}_3\text{H}:\text{AGU}$) or longer durations (such as 6.0 h) were also attempted in our experiments. However, under these conditions, the turbid suspensions containing nanocrystals was converted to a translucent solution, and a very small amount of gray particles after centrifugation was recovered. It indicated that under high sulfated agent concentrations and excessive sulfation reactions, the crystalline and chemical structures of CNs may be seriously destroyed and degraded as monosaccharide, and even induced carbonization. On the other hand, for the desulfation reaction the alkaline content should be carefully controlled in order to avoid the transformation of cellulose type I to type II. In our experiments, the surface sulfated moieties are removed under mild alkaline (NaOH)

conditions, that is maximum concentration of alkaline was only 2 mol/L (≤ 8 wt%). The yields of postsulfated and desulfated nanocrystals are shown in Table 1, which are in the range of 75–87 wt%.

To prove the reliability of the postsulfation and desulfation treatments for CNs used in this study, spectroscopic characterization was performed for all samples. From FTIR spectra (as shown in Figure 2), the peak located at 1033 cm^{-1} was followed, which was attributed to the stretching vibration of sulfated groups ($-\text{SO}_3$).³⁰ In comparison with pristine nanocrystals (CN-0), the magnitude of the peak gradually increased for postsulfated nanocrystals (solid lines in Figure 2), whereas it gradually decreased for desulfated nanocrystals (dot lines in Figure 2). These changes indicated the implementation of introducing gradient contents of sulfate groups on the surface of CNs samples.

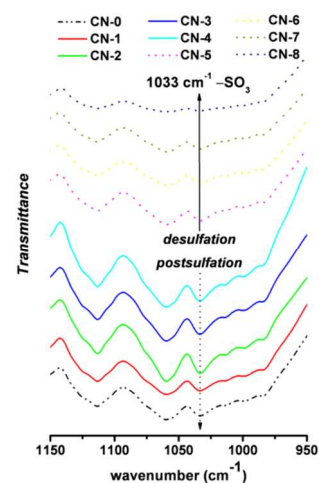


Fig. 2 FTIR spectra for various CNs samples with postsulfation or desulfation treatment in the wavenumber range 1150 to 950 cm^{-1} .

Surface postsulfation and desulfation of CNs were further analyzed by X-ray photoelectron spectroscopy, which was more accurate and objective. XPS can reveal the elements present in the sample, as well as determine the atomic and mass concentration of the elements. It provides a more quantitative idea for the level of surface modification. Figure 3 shows the general XPS spectra for pristine nanocrystals (CN-0), postsulfated nanocrystals (CN-4), and desulfated nanocrystals

Table 1. Yields of modified CNs samples after surface postsulfation and desulfation treatments; contents of sulfur %S (expressed as elemental sulfur by weight content) measured by elemental analysis; content of surface hydroxyl groups ($-\text{OH}$), sulfate groups ($-\text{OSO}_3^-$), and degree of substitution ($DS_{-\text{OSO}_3^-}$) for various CNs samples.

Samples	Yield		Elemental analysis			Surface $-\text{OH}$	Surface $-\text{OSO}_3^-$	$DS_{-\text{OSO}_3^-}$
	%	%	%S	%C	%O	mmol/g	mmol/g	%
CN-0	—	—	0.67	42.31	50.75		0.209	13.45
CN-1	86.21		0.77	42.21	50.64		0.241	15.51
CN-2	83.45		0.91	42.25	50.29		0.284	18.28
CN-3	82.76		1.09	42.16	50.40		0.341	21.94
CN-4	79.31		1.31	40.72	50.25	1.554	0.409	26.32
CN-5	87.93		0.53	42.01	51.46		0.166	10.68
CN-6	84.48		0.46	42.17	50.78		0.144	9.27
CN-7	81.03		0.29	42.47	50.97		0.0906	5.83
CN-8	75.86		0.18	42.49	51.22		0.0563	3.62

(CN-8), together with the signal assignments for sulfur (S2p, 165–168 eV) and sodium (Na1s, 1072 eV) elements. The intensity of the sulfur signal peak for the three samples was compared, and content ratio of sulfur to carbon (S/C) elements was calculated. It was shown that postsulfated nanocrystals (CN-4) possessed the maximum S/C ratio value, i.e. 5.4%; whereas desulfated nanocrystals (CN-8) had the lowest sulfur content, with the S/C ratio of 0.25%. As for sodium element, only CN-8 nanocrystal sample showed the signal of sodium with a Na/C ratio of 4.5%, which was the further proof for the desulfation treatment of CNs.

The weight contents of sulfur (S), carbon (C), and oxygen (O) elements in various CNs samples were measured by elemental analysis, and the data are shown in Table 1. The content of sulfur element in pristine nanocrystals (CN-0) was about 0.67%, which was close to the value reported in the previous report.¹⁹ Regarding the changes in sulfur content for postsulfated and desulfated nanocrystals, a logical tendency can be observed. In contrast to CN-0, the sulfur content for postsulfated nanocrystals CN-(1 to 4) and desulfated nanocrystals CN-(5 to 8) gradually increased up to a maximum value of 1.31%, and decreased to a minimum value of 0.18%, respectively. In fact, it was reported that during the biosynthesis process, trace amounts of sulfur remained in plant tissues, which can explain the presence of slight sulfur for CN-8 sample.²⁰

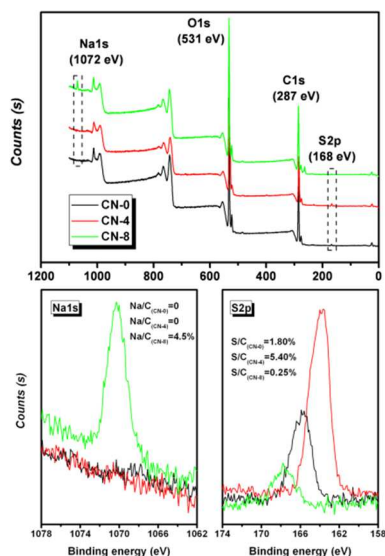


Fig. 3 General XPS spectra for pristine cellulose nanocrystals (CN-0), postsulfated cellulose nanocrystals (CN-4), and desulfated cellulose nanocrystals (CN-8) with signal assignments (sodium Na1s, sulfur S2p).

Morphological observation and dimensions.

Before discussion on CN surface chemistry, the morphology of nanocrystals should be checked, and the geometrical dimensions should be defined. AFM was used to observe the morphology and measure the dimensions of the nanoparticles. Figure 4 shows the amplitude, height and phase images from

AFM at different observation scales ($10 \times 10 \mu\text{m}$; $3.3 \times 3.3 \mu\text{m}$; $1.1 \times 1.1 \mu\text{m}$). It was shown that all CNs samples exhibited the typical and expected rod-like or needle-like morphology, with a length of about 100–300 nm, and width of about 10–30 nm. Interestingly, by comparing the three series images, it seemed that the dimensions of postsulfated nanocrystals CN-4 were more homogeneous, which may be associated to the enhanced electrostatic repulsion among nanoparticles in aqueous suspension.

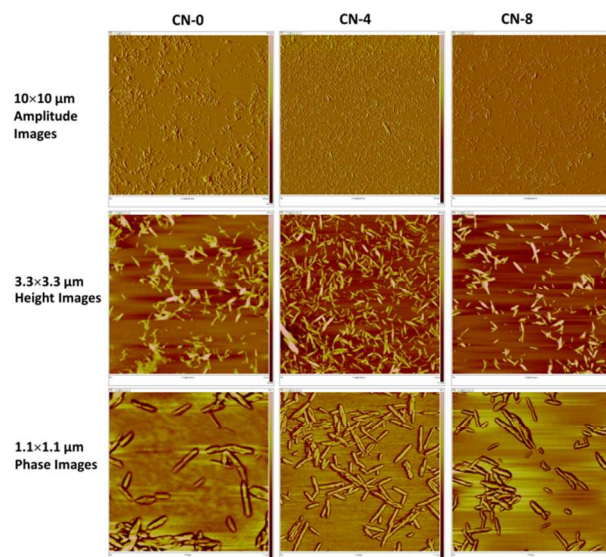


Fig. 4 AFM images for pristine cellulose nanocrystals (CN-0), postsulfated cellulose nanocrystals (CN-4), and desulfated cellulose nanocrystals (CN-8) at different observation scales.

Further statistical analysis of nanocrystal dimensions was performed by Nanoscope software. As representative samples, statistical analysis for dimensions and distribution determined from AFM images for samples CN-0, CN-4 and CN-8 are shown in Figure S1 and Figure S2 (*Supplementary Information*). Through the statistic measurements with over 100 individual nanocrystals from AFM images (mainly focusing on the images with the scale of $3.3 \times 3.3 \mu\text{m}$ and $1.1 \times 1.1 \mu\text{m}$), the average length (L), width (W) and height (H) of CNs were about 150 nm, 22 nm, and 5 nm, respectively. Specifically, pristine nanocrystals CN-0 showed a length of 169.9 ± 86.8 nm, width of 23.0 ± 8.9 nm, and height of 5.2 ± 1.9 nm; whereas postsulfated nanocrystals CN-4 exhibited a length of 152.0 ± 61.6 nm, width of 22.7 ± 8.7 nm, and height of 5.0 ± 1.3 nm; and desulfated nanocrystals CN-8 behaved a length of 148.6 ± 68.1 nm, width of 21.8 ± 8.9 nm, and height of 5.0 ± 1.5 nm. From the dimension changes, it was shown that the average length gradually decreased for modified nanocrystals because of the reduction of large scale nanocrystals. As shown in Figure S1, CN-0 nanocrystals with a length higher than 220 nm disappeared in CN-4 and CN-8 samples, which can be attributed to the further removal of amorphous region during the postsulfation and desulfation treatments. Geometrical dimension data for all nine CNs samples are summarized in Table 2. The nanoscaled dimension and distribution of cotton

CNs demonstrate that these nanoparticles have the promising potential to be used as rigid nano-reinforcing filler for composites.

XRD (One black bar represents a glucan chain, and green bars are surface available glucan chains); (c) chemical conformation and dimensions of one single cellobiose unit.

Table 2. Geometrical dimensions, values of crystallinity index (χ_c) and crystalline dimensions (B_{200} , $B_{1\bar{1}0}$ and B_{110}), and ζ -potentials for various CNs samples from the results of AFM, XRD, and zeta-potential analysis.

Sample	Geometrical dimension (nm)			χ_c %	Crystalline dimension (nm)			ζ -potential mV
	Length	Width	Height		B_{200}	$B_{1\bar{1}0}$	B_{110}	
CN-0	169.9±86.8	23.0±8.9	5.2±1.9	88.6	6.8	5.3	6.6	-40.4±1.7
CN-1	159.5±67.4	22.3±10.4	5.3±2.0	88.1	6.7	5.3	6.5	-47.8±1.9
CN-2	154.1±57.9	21.7±7.9	5.1±1.8	88.2	6.8	5.3	6.6	-54.8±2.2
CN-3	154.6±69.2	22.3±9.7	5.2±1.5	88.5	6.8	5.3	6.5	-61.7±2.4
CN-4	152.0±61.6	22.7±8.7	5.0±1.3	88.0	6.7	5.3	6.7	-66.1±1.5
CN-5	157.6±71.3	23.6±10.1	5.1±1.7	87.1	6.7	5.2	6.7	-32.8±2.3
CN-6	150.6±64.8	21.9±8.7	5.1±1.6	88.0	6.8	5.2	6.7	-27.6±1.4
CN-7	151.6±69.5	22.6±9.4	5.1±1.4	87.5	6.7	5.3	6.6	-17.9±1.1
CN-8	148.6±68.1	21.8±8.9	5.0±1.5	88.2	6.8	5.3	6.7	-7.4±0.8

Morphology models and surface chemistry of cellulose nanocrystals.

The degree of substitution (DS) of surface hydroxyl groups ($-OH$) replaced by sulfate groups ($-OSO_3^-$) can be calculated according to Eq. (4). In this equation, $n_{-OSO_3^-}$ represents the mole fraction of sulfate groups, which can be calculated according to Eq. (5) from the results of elemental analysis. The amount of surface ($-OH$) on CNs [$n_{surface(-OH)}$] can be deduced from some fundamental models (as shown in Figure 5 a, b, c), and calculated from Eq. (6).

$$DS = \frac{n_{-OSO_3^-}}{n_{surface(-OH)}} \quad (4)$$

$$n_{-OSO_3^-} = n_S = \frac{m_S}{M_S} = \frac{m_{CN} S\%}{M_S} \quad (5)$$

$$n_{surface(-OH)} = N_0 \cdot A_{total(CN)} \quad (6)$$

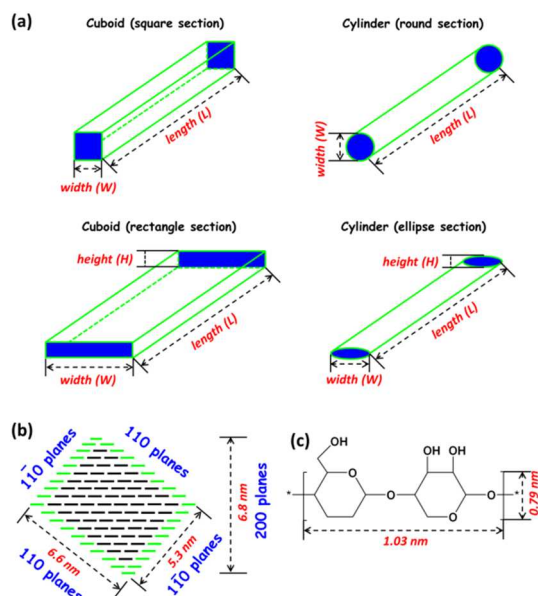


Fig. 5 Schematic models of (a) an individual rod-like cellulose nanocrystal and dimensions (cuboid shape with square section; cylinder shape with round section; cuboid shape with rectangular section; cylinder shape with ellipsoid section); (b) an idealized elementary crystallite region for cotton cellulose nanocrystal from the analysis of

According to previous reports,^{20,31} the representative elementary crystallite region of cotton CN is proposed (model b), which exhibits a square or parallelogram section with 10×10 glucose units based on the d -spacing of (110), ($1\bar{1}0$), and (200) planes and its size is roughly $5.3 \text{ nm} \times 6.6 \text{ nm}$. Crystalline dimensions for three planes can be obtained from XRD experiments, and the data are summarized in Table 2. (Further discussion on the effect of sulfate groups on crystalline properties of CNs will be provided in next part.) Taking hydroxyl groups and length of cellobiose unit into consideration (model c), 36 glucan chains are located on the surface of the crystal, which correspond to 120 available hydroxyl groups. Consequently, the number of hydroxyls per unit surface area (N_0) on cotton cellulose nanocrystal can be calculated as $8.13 \times 10^{-3} \text{ mmol/m}^2$ according to Eq. (7).

$$N_0 = \frac{120 (-OH)}{N_A (2A_{110} + 2A_{1\bar{1}0})} \quad (7)$$

In Eq. (7),

$$A_{110} = 6.6 \times 1.03 \text{ nm}^2$$

$$A_{1\bar{1}0} = 5.3 \times 1.03 \text{ nm}^2$$

$$N_A = 6.02 \times 10^{23} \text{ (Avogadro's number)}$$

Consequently, to determine the amount of surface $-OH$ on CNs, the key point is to calculate the value of the total specific surface area [$A_{total(CN)}$], which can be calculated from Eq. (8). In this equation, $\rho_{cellulose}$ is the density of cellulose (1.50 g/cm^3); $A_{single(CN)}$ and $V_{single(CN)}$ represent the surface area and volume of a single nanocrystal, respectively.

$$A_{total(CN)} = \frac{m_{CN}}{\rho_{cellulose}} \cdot \frac{A_{single(CN)}}{V_{single(CN)}} \quad (8)$$

Interestingly, with different cross-section models, the results of $A_{total(CN)}$ will be completely different. Generally, cellulose nanocrystal can be considered as a kind of rod-like or needle-like nanoparticle, so the simplest cross-section model is cuboid or cylinder with the square or round bottom, as shown in model (a). However, in this study, according to AFM observations, the width and height of CNs are different ($W=22 \text{ nm}$, and $H=5 \text{ nm}$), which indicates that the cuboid or cylinder model for the nanocrystal may be more reasonable. Four kinds of cross-

section models for rod-like CNs, viz. square, round, rectangular and ellipsoid models, are shown in model (a) of Figure 5. The CNs dimensions, length (L), width (D) and height (H), can be obtained from AFM observation summarized in Table 2.

If choosing the **cuboid model (square section)** for CN,

$$A_{\text{single}(CN)} = 4WL$$

$$V_{\text{single}(CN)} = W^2L$$

So, in Eq. (8):

$$A_{\text{total}(CN)} = \frac{m_{CN}}{\rho_{\text{cellulose}}} \cdot \frac{4}{W} \quad (8-1)$$

If choosing the **cylinder model (round section)** for CN,

$$A_{\text{single}(CN)} = \pi WL$$

$$V_{\text{single}(CN)} = \pi W^2L/4$$

So, in Eq. (8):

$$A_{\text{total}(CN)} = \frac{m_{CN}}{\rho_{\text{cellulose}}} \cdot \frac{4}{W} \quad (8-2)$$

If choosing the **cuboid model (rectangular section)** for CN,

$$A_{\text{single}(CN)} = 2(W + H)L$$

$$V_{\text{single}(CN)} = WHL$$

So, in Eq. (8):

$$A_{\text{total}(CN)} = \frac{m_{CN}}{\rho_{\text{cellulose}}} \cdot \frac{2(W + H)}{WH} \quad (8-3)$$

If choosing the **cylinder model (ellipsoid section)** for CN,

$$A_{\text{single}(CN)} = [2\pi H + 4(W - H)]L$$

$$V_{\text{single}(CN)} = \pi LHW$$

So, in Eq. (8):

$$A_{\text{total}(CN)} = \frac{m_{CN}}{\rho_{\text{cellulose}}} \cdot \frac{2\pi H + 4(W - H)}{\pi WH} \quad (8-4)$$

Interestingly, it is observed that the values for $A_{\text{total}(CN)}$ using square and round section models show the same results (Eq. 8-1 and 8-2), depending on the width (W) of the nanocrystal only; whereas the values for $A_{\text{total}(CN)}$ using rectangular and ellipsoid section models depend on both the width (W) and height (H) (Eq. 8-3 and 8-4).

Data for total specific surface area [$A_{\text{total}(CN)}$], amount of $n_{\text{-OSO}_3^-}$ and $n_{\text{surface(-OH)}}$, and degree of substitution (DS) of sulfate groups for CN-0 were calculated based on the different cross-section models, and are summarized in Table 3. It is shown that if square or round models are chosen for cotton CNs, more than 20% of surface hydroxyl groups have been substituted by sulfate groups during the H_2SO_4 -esterification hydrolysis, which indicates that most of active hydroxyl groups located on C-6 have been replaced. Therefore, from these two models, desulfation treatment for H_2SO_4 -hydrolyzed CNs is necessary before chemical modification. However, if choosing rectangle model for CNs, only 7.9% (only about 1/3 of the value for square or round models) surface hydroxyl groups is substituted during the H_2SO_4 -hydrolysis, and a large amount of active hydroxyl groups have been remained.

In this study, ellipse model for the CNs cross-section is also proposed, and the DS value of sulfate groups for nine CNs samples is shown in Table 1. Specifically, if ellipse model is

chosen, about 13% of the surface hydroxyl groups are substituted by sulfate groups during hydrolysis for pristine nanocrystal CN-0. The maximum DS value is about 26% for CN-4, which indicates that 1/4 of the hydroxyl groups on the CN surface can be replaced by sulfate groups during the postsulfation treatment.

Table 3. Total specific surface area [$A_{\text{total}(CN)}$], amount of sulfate groups [$n_{\text{-OSO}_3^-}$] and surface hydroxyl groups [$n_{\text{surface(-OH)}}$], and degree of sulfation substitution (DS) for CN-0 calculated from different cross-section models.

Model	$A_{\text{total}(CN)}$	Surface – OH	Surface – OSO_3^-	$DS_{\text{-OSO}_3^-}$
	m^2	mmol/g	mmol/g	%
Square/Round	117.5	0.955		21.88
Ellipse	191.2	1.554	0.209	13.45
Rectangle	325.4	2.646		7.90

The proposal of ellipse model for cotton CNs is based on AFM observation and presumption of cross-section shape. Figure 6 presents the orthography image of CNs. However, due to the small scale of height dimension (about 5 nm), it was difficult to directly observe and determine the end shape of nanocrystals. With the enlargements of height to ten, thirty, and fifty times ($\times z$ axis), some interesting changes appeared on AFM images. As indicated by the green and blue circles in Figure 6, it seems that after enlargement, the shape of CNs cross-section transformed to “mountain” with a peak on the top. If the nanocrystal cross-section is rectangular, the size from top to bottom should keep invariability during the height enlargement; whereas ellipsoid cross-section was suitable for this change. Although the ellipse cross-section model should be further validated by other observation techniques,³² it is a new choice to be used for the analysis of CNs surface chemistry.

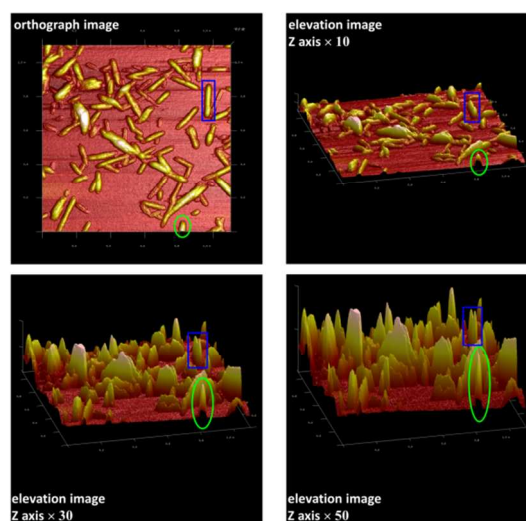


Fig. 6 AFM image analysis for the observation of cross-section shape for cellulose nanocrystals (CN-4).

Effect of sulfate groups on the properties of cellulose nanocrystals.

Besides the surface chemistry discussed above, different sulfate group contents on the surface of CNs should also significantly affect their physical properties, such as crystalline structure and thermal stability for inherent nanocrystal, and birefringence behavior and rheological behavior for nanocrystal suspensions. Some studies have reported the influence of sulfate groups on the rheological behavior of CNs suspensions. For instance, it was reported that the introduction of more sulfate groups on the surface of CNs drastically reduced the viscosity of the suspension and removed the time dependence.³³ Recently, it was found that the sulfation degree of CNs has a significant effect on the critical concentration at which transitions from isotropic to liquid crystal and liquid crystal to gel occur.³⁴ It is a pity that some inconsistent conclusions on the effect of sulfate groups were given in different studies, such as thermal stability of sulfated CNs as mentioned in the Introduction Section. In this study, important physical properties of CNs possibly affected by the sulfate group content have been further investigated. Because of the wide range and detailed sulfate group contents (nine samples from minimum to maximum contents), the global trend analysis on properties for sulfated CNs would be more reasonable.

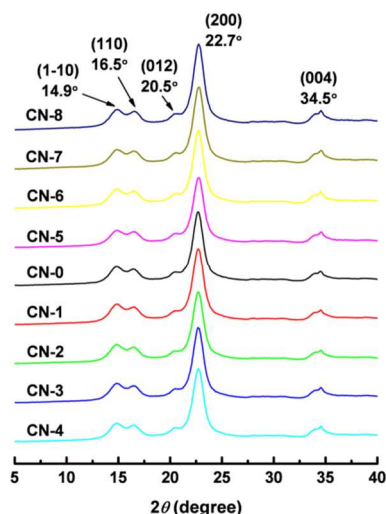


Fig. 7 X-ray diffraction patterns for various cellulose nanocrystals with different surface sulfate group contents.

Crystal properties are among the most important physical properties of CNs, which can reflect the integrity of the original structure of the nanocrystals. The degree of postsulfation should be carefully controlled to react only on the surface of CNs, in order to maximally introduce sulfate groups and avoid the further structural destruction. On the other hand, due to the use of alkaline solution for desulfation treatment, the polymorphic and chemical transformation of cellulose (such as type I for cotton cellulose in this study) must be prevented. XRD is the common technique for the investigation of crystalline structure of cellulose. The X-ray diffraction patterns for the various CNs with different surface sulfate group contents are shown in Figure 7, and the values of the crystallinity index (χ_c) and crystalline dimensions are

summarized in Table 2. The similar patterns and intensity preservation of diffraction peaks for all samples indicated that the postsulfation and desulfation treatments did not destroy or convert the inherent crystalline structure of nanocrystals. Indeed, the characteristic diffraction peaks at 2θ angles around 14.9° , 16.5° , 20.5° , 22.7° , 34.5° assigned to the typical reflection planes of cellulose I, $1\bar{1}0$, 110 , 012 , 200 , 004 , respectively, were preserved.³⁵ The crystallinity index (χ_c) of CNs were calculated according to the Segal method (Eq. 2),³⁶ which exhibited a high crystallinity (about 88% for χ_c) and maintenance of the crystalline structure. From the calculation according to Scherrer equation (Eq. 3), the crystalline dimensions of different planes (B_{200} , $B_{1\bar{1}0}$ and B_{110}) for CNs samples can be obtained. As shown in Table 2, the sizes of 200 , $1\bar{1}0$, and 110 planes for cotton CNs were about 6.8 nm, 5.3 nm, and 6.6 nm, which was consistent with the parallelogram elementary crystallite model proposed in Figure 5b. On the basis of XRD results, it can be stated that the contents of surface sulfate groups do not obviously affect or have less influence to the crystal properties of CNs.

Owing to the presence of sulfate groups on their surface, rod-like CNs changed to negatively charged nanoparticles. In the colloidal system of sulfated CNs, the dispersion medium and the stationary layer of fluid attached to the dispersed nanoparticles will provide the potential difference, which is named zeta potential (ζ -potential). The value of zeta potential is related to the stability of the colloidal dispersion, and indicates the degree of repulsion between adjacent, similarly charged particles in a suspension. The effect of sulfate groups on ζ -potential of CNs is presented in Table 2. With the increase of sulfate group content, sulfated CNs possessed a more negative surface, and exhibited lower ζ -potential values. Especially for postsulfated nanocrystals sample CN-4, the value of ζ -potential reached to -66.1 ± 1.5 mV, which indicated the strong repulsive force between nanoparticles, and therefore the promotion of its dispersion in suspension (as proved by AFM). It is worth noting that desulfation treatment for sulfated nanocrystals was also effective, which can be reflected by the significant increase of ζ -potential for desulfated CNs samples.

Thermal stability is another important physical property for CNs, which plays a critical role in the preparation of melt processed CNs-reinforced composites. As mentioned in the Introduction Section, the effect of sulfate groups on the surface of CNs to thermal stability was led to inconsistent conclusions from different reports. Therefore, thermal degradation behavior of sulfated CNs is further investigated by thermogravimetric analysis in this study, which is shown in Figure 8. Interestingly, in comparison with all nanocrystal samples, native cotton exhibited the highest thermal stability for the first phase of thermal decomposition (T_{d1}). Because of the hydrolysis and presence of sulfate groups, the values of T_{d1} for all postsulfated nanocrystals sharply decreased to about 150°C compared with native cotton. By determining T_{d1} for postsulfated CNs themselves (event a in Figure 8), it appears that more sulfate groups on nanocrystals induced a lowering of T_{d1} , such as the decrement (Δt_1) of 12.3°C from CN-1 to CN-4 samples. In

contrast to postsulfated nanocrystals, the values of T_{d1} for desulfated CNs generally enhanced about 100 °C attributed to the removal of sulfate groups and presence of sodium on nanocrystals. From the analysis of T_{d1} for desulfated CNs themselves (event b in Figure 8), similar conclusion can be obtained, i.e. less sulfate groups on nanocrystals resulted in higher T_{d1} , such as the increment (Δt_2) of 13.8 °C from CN-5 to CN-8 samples. It should be pointed out that according to our investigation, besides sulfate groups, the introduction of sodium on the surface of CNs may be another factor that significantly affects their thermal property. Furthermore, from the TGA thermograms in Figure 8, thermal degradation behavior of cellulose for the second phase of thermal decomposition (T_{d2}) can also be observed. Differently, all nanocrystal samples possessed higher T_{d2} values than native cotton (about 65 °C), which may be associated to the higher crystallinity for nanocrystal samples.

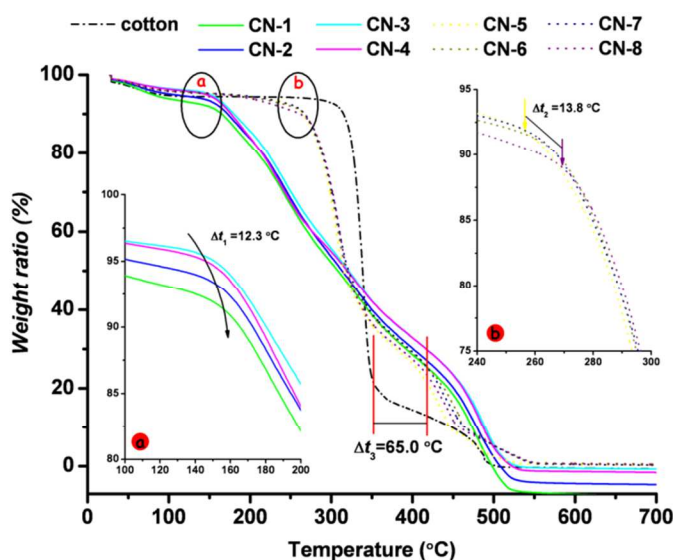


Fig. 8 Effect of surface sulfate groups on the thermal stability of cellulose nanocrystals (TGA thermograms).

In 1959, the birefringence character of acid-treated cellulose and chitin crystallites was first reported,³⁷ which was the behavior through strong adsorption of one of polarized rays to possess two refractive indices. Birefringence of CN suspensions can be observed with two linear polarizers crossed at 90° (cross-nicols or crossed-polars), and gives a quick indication of the successful preparation of well-dispersed CNs suspensions. Figure 9 shows the photographs of aqueous suspensions of various CNs with postsulfation and desulfation treatments. The presence of negative charges ($-OSO_3^-$) on CNs surface induced an electrostatic repulsion between nanoparticles, and the suspensions exhibited the formation of birefringence domains. Because of the stable dispersion and flow anisotropy from alignment of nano-rods under flow state, the birefringence character for postsulfated nanocrystal suspensions was maintained. With the desulfation and progressive removal of sulfate groups, nanoparticles in suspensions tended to aggregate, which induced the reduction and weakening of

birefringence domains. Especially for strongly desulfated nanocrystals, samples CN-7 and CN-8, the birefringence behavior of suspensions was difficult to be observed.

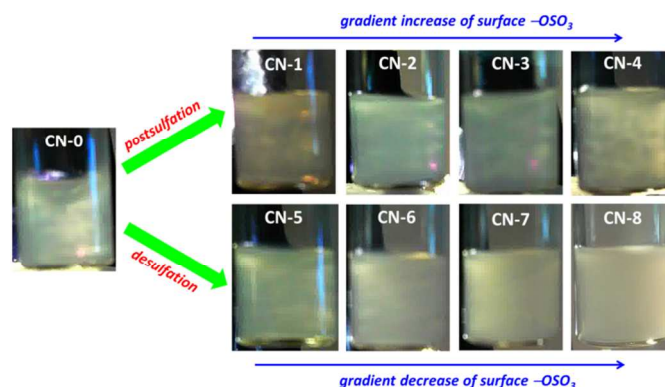


Fig. 9 Photographs of aqueous suspensions of various cellulose nanocrystals viewed through cross polarizers (0.5 wt%).

Conclusions

The objective of this study is to investigate how surface sulfate groups affect the surface chemistry and physical properties of cellulose nanocrystals. Through the regulation of reactant ratios and reactive conditions for postsulfation and desulfation, gradient contents of sulfate groups can be introduced on the surface of CNs. Based on the discussion of nanocrystal's surface chemistry, the influence of different cross-section models for the calculation of substitution degrees of sulfate group was investigated, and a new ellipsoid model for cotton CNs was proposed on the basis of AFM observation. Finally, the effects of sulfate groups on diverse properties of CNs and their suspensions have been discussed, and some issues with inconsistent conclusions from previous reports were further validated. Future studies will focus on the electrostatic interactions between negative charges from sulfated CNs and positive charges from cationic polymers or molecules. With the detection and measurement of electrostatic interactions, it is expected to reveal the strength and mechanism of this special interaction from coupling charges and therefore advance the application of CNs electrostatic grafting.

Acknowledgements

The authors are grateful to Mrs. Cécile Sillard (LGP2, Grenoble INP-Pagora) for the help in AFM observation. This work is supported by the China Scholarship Council (CSC) under Grant No. 2011695007.

Notes and references

Address: Grenoble Institute of Technology (Grenoble INP) –The International School of Paper, Print Media and Biomaterials (Pagora), CS10065, 38402 Saint Martin d'Hères Cedex, France.

Tel.: +33 476826995. Fax: +33 476826933.

E-mail: Alain.Dufresne@pagora.grenoble-inp.fr

† Electronic Supplementary Information (ESI) available: **Figure S1.** Size statistics for length (L) and width (W) from AFM images for cellulose nanocrystal samples (CN-0, CN-4 and CN-8); **Figure S2.** Size statistics

- of height (H) for cellulose nanocrystals samples (CN-0, CN-4 and CN-8) with the analysis of NanoScope software. See DOI: 10.1039/b000000x/
- 1 A. Dufresne, Nanocellulose. From nature to high performance tailored materials; Walter de Gruyter GmbH: Berlin and Boston, MA; 2012.
 - 2 The global market for nanocellulose to 2017; Futures Markets Inc.: Edinburgh, Lothian EH74NA, United Kingdom, 2012.
 - 3 L. Brinchi, F. Cotana, E. Fortunati and J. M. Kenny, *Carbohydr. Polym.*, 2013, **94**, 154–169.
 - 4 J. Araki, *Soft Matter*, 2013, **9**, 4125–4141.
 - 5 A. Dufresne, *Mater. Today*, 2013, **16**, 220–227.
 - 6 A. C. W. Leung, E. Lam, J. Chong, S. Hrapovic and J. H. T. Luong, *J. Nanopart. Res.*, 2013, **15**, 1636 (24 pages).
 - 7 N. Lin, J. Huang and A. Dufresne, *Nanoscale*, 2012, **4**, 3274–3294.
 - 8 P. Tingaut, T. Zimmermann and G. Sèbe, *J. Mater. Chem.*, 2012, **22**, 20105–20111.
 - 9 E. Lam, K. B. Male, J. H. Chong, A. C.W. Leung and J. H.T. Luong, *Trends Biotechnol.*, 2012, **30**, 283–290.
 - 10 Y. Habibi, L. A. Lucia and O. J. Rojas, *Chem. Rev.*, 2010, **110**, 3479–3500.
 - 11 B. G. Rånby, *Acta Chem. Scand.*, 1949, **3**, 649–650.
 - 12 E. D. Cranston, D. G. Gray and M. W. Rutland, *Langmuir*, 2010, **26**, 17190–17197.
 - 13 C. Moreau, N. Beury, N. Delorme and B. Cathala, *Langmuir*, 2012, **28**, 10425–10436.
 - 14 S. Y. Liew, W. Thielemans and D. A. Walsh, *J. Phys. Chem. C*, 2010, **114**, 17926–17933.
 - 15 H. Ma, C. Burger, B. S. Hsiao and B. Chu, *Biomacromolecules*, 2012, **13**, 180–186.
 - 16 W. Thielemans, C. R. Warbey and D. A. Walsh, *Green Chem.*, 2009, **11**, 531–537.
 - 17 F. Jiang, J. D. Kittle, X. Tan, A. R. Esker and M. Roman, *Langmuir*, 2013, **29**, 3280–3291.
 - 18 I. Kalashnikova, H. Bizot, B. Cathala, and I. Capron, *Biomacromolecules*, 2012, **13**, 267–275.
 - 19 T. Abitbol, E. Kloser and D. G. Gray, *Cellulose*, 2013, **20**, 785–794.
 - 20 J. Gu, J. M. Catchmark, E. Q. Kaiser and D. D. Archibald, *Carbohydr. Polym.*, 2013, **92**, 1809–1816.
 - 21 M. Roman and W. T. Winter, *Biomacromolecules*, 2004, **5**, 1671–1677.
 - 22 M. I. Voronova, O. V. Surov and A. G. Zakharov, *Carbohydr. Polym.*, 2013, **98**, 465–469.
 - 23 N. Lin and A. Dufresne, *Macromolecules*, 2013, **46**, 5570–5583.
 - 24 K. Zhang, E. Brendler, A. Geissler and S. Fischer, *Polymer*, 2011, **52**, 26–32.
 - 25 Z.-M. Wang, L. Li, K.-J. Xiao and J.-Y. Wu, *Bioresource Technol.*, 2009, **100**, 1687–1690.
 - 26 F. Jiang, A. R. Esker and M. Roman, *Langmuir*, 2010, **26**, 17919–17925.
 - 27 E. Kloser and D. G. Gray, *Langmuir*, 2010, **26**, 13450–13456.
 - 28 M. Hasani, E. D. Cranston, G. Westman and D. G. Gray, *Soft Matter*, 2008, **4**, 2238–2244.
 - 29 O. van den Berg, J. R. Capadona and C. Weder, *Biomacromolecules*, 2007, **8**, 1353–1357.
 - 30 S. Suganuma, K. Nakajima, M. Kitano, D. Yamaguchi, H. Kato, S. Hayashi and M. Hara, *J. Am. Chem. Soc.*, 2008, **130**, 12787–12793.
 - 31 S. Elazzouzi-Hafraoui, Y. Nishiyama, J.-L. Putaux, L. Heux, F. Dubreuil and C. Rochas, *Biomacromolecules*, 2008, **9**, 57–65.
 - 32 J. Majoinen, J. S. Haataja, D. Appelhans, A. Lederer, A. Olszewska, J. Seitsonen, V. Aseyev, E. Kontturi, H. Rosilo, M. Österberg, N. Houbenov and O. Ikkala, *J. Am. Chem. Soc.*, 2014, **136**, 866–869.
 - 33 J. Araki, M. Wada and S. Kuga, *J. Wood. Sci.*, 1999, **45**, 258–261.
 - 34 S. Shafiei-Sabet, W. Y. Hamad and S. G. Hatzikiriakos, *Rheol. Acta.*, 2013, **52**, 741–751.
 - 35 N. Lin, C. Bruzzese and A. Dufresne, *ACS Appl. Mater. Interfaces*, 2012, **4**, 4948–4959.
 - 36 L. Segal, J. J. Creely, A. E. Martin and C. M. Conrad, *Text. Res. J.*, 1959, **29**, 786–794.
 - 37 R. H. Marchessault, F. F. Morehead and N. M. Walter, *Nature*, 1959, **184**, 632–633.